Systems and Strategies for Accessing the Information Content of fNIRS Imaging in Support of Noninvasive BCI Applications

Randall L. Barbour[1,2], Harry L. Graber[1,2], Yong Xu[1,2], Yaling Pei[2], Glenn R. Wylie[3], Gerald T. Voelbel[3], John DeLuca[3], and Andrei V. Medvedev[4]

[1] Department of Pathology, SUNY Downstate Medical Center, Brooklyn, NY, 11203
[2] NIRx Medical Technologies, Glen Head, NY, 11545
[3] Kessler Foundation Research Center, W. Orange, NJ, 07101
[4] Center for Functional and Molecular Imaging, Georgetown University Medical Center, Washington, DC, 20057
{randall.barbour, harry.graber, yong.xu}@downstate.edu, ypeinirx@gmail.com, {gwylie, gvoelbel, jdeluca}@kesslerfoundation.net, am236@georgetown.edu

Abstract. An essential component for a practical noninvasive brain-computer interface (BCI) system is data recording technology that can access the information-processing activity of the brain with high fidelity and throughput. Functional near-infrared spectroscopic (fNIRS) imaging is a methodology that shows promise in meeting this need, having a demonstrated sensitivity to both the slow hemodynamic response that follows neuroactivation and to the lower amplitude fast optical response that is considered a direct correlate of neuroactivation. In this report we summarize the technology integration strategy we have developed that permits detection of both signal types with a single measuring platform, and present results that document the ability to detect these data types transcranially in response to two different visual paradigms. Also emphasized is the effectiveness of different data analysis approaches that serve to isolate signals of interest. The findings support the practical utility of NIRS-based imaging methods for development of BCI applications.

Keywords. Diffuse Optical Tomography, fNIRS imaging, fast signal, combinatorial Hb States, Neuroactivation, Visual Stimulus, NIRS Technology.

1 Introduction

There are many examples where the detailing of the internal properties of otherwise opaque materials has significant value. In the late nineteen eighties, SUNY investigators first recognized that even in the limit where the penetrating energy is diffusely scattered, useful images of the internal properties of these materials was nevertheless possible [1,2]. A principal application area considered at that time for this type of imaging was the use of near infrared (NIR) light to study the optical properties of tissue [3]. Documented was the ability to generate 3D tomographic images of diffusing media whose dimensions have clinical interest based on physical models of light trans-

port [4,5]. These preliminary findings have gone on to spur the development of a new investigative field known by the name of Diffuse Optical Tomography (DOT), or, alternately, NIRS imaging.

In the ensuing years, much effort has been directed to delineating the cost/performance trade-offs of different sensing strategies for data collection, techniques applied to forming tomographic images of diffusely scattering media, and different methods for extracting useful information from these images.

Advantages of NIRS studies include good tissue penetration, exceptional sensitivity to the hemoglobin (Hb) signal, and recovery of 3D images having a spatial resolution on the order of 1 cm. Other favorable attributes include excellent temporal resolution (msec-sec range), information about all Hb components, ease of use in different environments (including freely moving subjects), and low system cost.

Practical imaging system development is essentially an optimization problem whose limits are defined by application needs and cost/performance constraints. Typical parameters include details of the sensor array, acquisition speed and sensitivity, system control and calibration, validating phantoms, and, increasingly, access to sophisticated computing environments that support reliable feature extraction. Below we briefly outline system design strategies our group has implemented to meet these various needs, and follow this with results from experimental studies that document the capability of these designs to explore different elements of the response to neuroactivation.

1.1 Light Sensing Strategies. Brain function in the adult can be usefully probed by NIRS imaging techniques to a maximum depth of approximately 3 cm. Separation of superficial from deeply lying structures requires sampling of backreflected light using fiber-coupled sensors positioned both near and far from any source. Because fast data collection is needed to capture dynamic phenomena (*e.g.*, cerebral response to stimuli), our approach has been to employ dense sensor arrays that also have large a dynamic range of measurement. Rapid scanning is achieved by using a fast optical switch that can be operated to support all or only one of the available illumination sites. The latter arrangement allows for parallel sampling of the entire sensor array (currently up to 128 sensors) at speeds of 70-140 Hz, depending on type of signal handling circuitry. Measurements are performed using frequency-encoding techniques with homodyne detection in the audio-frequency range to allow for separate detection of light intensities from multiple illuminating wavelengths [6-8].

Tomography studies typically are conducted using a time-multiplexed, multi-site illumination approach wherein the full array is read for each illuminating site [1,3,4,6-8]. Currently feasible are illumination/sensing approaches that support sampling from four arrays in parallel, each supporting a 32S × 32D array and up to six wavelengths (4,096 illumination-detection pairs per wavelength per image frame). Such configurations can allow for tomographic imaging of approximately half the surface area of the cranium. Full head coverage can be achieved using more sparsely spaced sensor arrays. This reduces the tomography capability to a surface mapping technique known in the scientific literature as Optical Topography [9,10]. By achieving spatial separation of light signals in three dimensions, the tomography method can be expected to yield findings with greater specificity.

1.2 Sensor Head Design. The presence of hair can be an important consideration in sensor head design. Dark hair can be strongly attenuating and in such cases, to enable good fiber coupling to the scalp, careful displacement of hair is needed to achieve good signal quality. We have implemented two different design solutions. One employs open scaffolding that allows attachment of arcs that serve to mechanically support spring-loaded optical fibers. The other is a head-shaped silicone membrane that supports placement of fibers within a nearly regular array. In our experience the former is best suited for subjects with dense hair, the latter where the expected impact of hair is less important.

1.3 Anatomical Mapping. In many instances, an important object of study is to map information gained from the imaging studies to the underlying anatomy. This requires knowledge of individual head shape, of the position of the sensor array with respect to this head shape, and specification of an appropriate atlas. Currently a variety of surface-rendering tools are commercially available that have modest complexity and cost. Using methods originally developed to map EEG findings [11], we have adopted these tools to allow for mapping of NIRS image findings.

The usual case for NIRS imaging, wherein mapping of *tomographic* findings to an atlas is desired, is more complex than is typical of EEG. A key component is the need for library files that support computation of tomographic images based on a wide range of possible sensor configurations. Our approach has been to introduce a GUI that allows for easy specification of selected array configurations. The considered files are themselves based on tessellations of a segmented 3D MRI map of an adult head. Fiducial measures, along with use of affine interpolation methods, allow for accurate mapping of the sensor array to this selected atlas. Mapping to other atlases, including the individual's MRI map, is also available.

1.4 Data Analysis. Many approaches used for analysis of NIRS data for neuroimaging studies are analogues of methods developed for fMRI. Useful endpoints fall into three classes: studies on resting states, localization of activated regions, and identification of regions that are functionally connected. Because of the strong dependence of signal quality on optode separation, the quality of data across the sensor array can vary greatly. This presents the need for preprocessing schemes wherein channels having poor signal quality can be excluded from subsequent analysis [7,8].

Preprocessing is followed by use of efficient 3D image reconstruction methods that are insensitive to the usual uncertainties of experiments [12-14]. While computationally efficient, these methods tend to produce images whose accuracy and resolution can be improved using more computationally intensive techniques. The latter methods, however, have severe practical limitations when applied to image time-series studies. To this end, we have implemented alternative image correction methods that have good performance and efficiency [15-20].

1.4.1 Signal Separation Methods. Many measures from intact systems constitute a complex mixture of information over space and time. In the case of NIRS, information is convolved spatially, on a macroscopic scale, because of scattering, and temporally because of coincident phenomenology affecting different elements of the vascular tree. Compared to topographic imaging methods, image reconstruction using model-based techniques provides an objective basis for effectively reducing the blurred paths of light in tissue caused by scattering [1-5,12-20].

Among the temporal decomposition methods are techniques that can provide for isolation of signals that are uncorrelated and independent [21,22]. These methods have found favor in the functional neuroimaging community because many of the applied stimulus paradigms produce responses that largely meet these criteria. Nevertheless, because biological systems tend to operate in ways less favorable to simplifying mathematics, in many instances strict interpretation of the deconvolved time series can prove difficult. Regardless, when applied with care, these methods can prove useful and, as shown later, we have adopted one class of ICA methods to isolate the fast optical signal.

1.4.2 Separation of Correlated Hemodynamic Signals. A specific data analysis strategy that we have applied to NIRS neuroimaging studies follows from the consideration that while there can be a time lag between an O_2 demand-linked "cause" and the subsequent blood-delivery "effect," still it is reasonable to associate different combinations of Hb levels with different conditions of balance or imbalance between the utilization and supply of O_2. For example, if Hb_{deoxy} is elevated and at the same instant Hb_{oxy} and Hb_{total} levels are reduced (in all cases, compared to their time-averaged levels in a resting baseline condition), we would interpret this as indicating that the tissue is in a state of net O_2 demand that the vasculature has not (yet) responded to by increasing the inflow of oxygenated blood. In like manner we derive the complete set of discrete combinatorial states defined in Table 1, each corresponding to a different pattern of Hb-level deviations from their baseline values in accordance with a neuroactivation induced supply-demand imbalance model.

Table 1. Definitions of discrete states used to characterize hemodynamic responses. Plus sign (+) denotes an instantaneous Hb level greater than the temporal mean value; minus sign (-) denotes an instantaneous level less than the temporal mean value.

	State 1	State 2	State 3	State 4	State 5	State 6
Hb_{oxy}	-	-	-	+	+	+
Hb_{deoxy}	-	+	+	+	-	-
Hb_{total}	-	-	+	+	+	-
	Balanced	Uncompensated O_2 debt	Compensated O_2 debt	Balanced	Uncompensated O_2 excess	Compensated O_2 excess

1.5 Data Analysis Examples. In the following sections we present illustrative examples of results that have been obtained by applying an ICA algorithm to one set of NIRS imaging data, and the combinatorial state analysis to another. Common to both measurements was that a visual sensory input was used to stimulate neural activations with a prescribed time course. The distinction that determines which analysis approach is the appropriate one is that in one case a single illumination site was used (~75 Hz framing rate), and time-multiplexed, multi-site illumination (~2 Hz) was

used in the other. For the first data set, ICA was used to identify the event-related fast optical signal, since it was expected that this signal would be independent of other sources of spatiotemporal variance in the data. The combinatorial-state decomposition was applied to the slow hemodynamic response data collected in the second experiment, where independence among the Hb components was not expected.

2 Methods

2.1 Data Collection

For both experiments, a multi-channel continuous wave near-infrared optical tomography imager (www.nirx.net) was used to measure, at multiple positions on each participant's scalp, the intensity of backreflected NIR light at 760 nm and 830 nm wavelengths. The optodes were positioned to make contact with the scalp, with ~1-cm inter-optode spacing, using an adjustable helmet with an open scaffolding design [23].

For the fast optical-response measurement, a 15-optode (3×5) array was positioned on the left side of the forehead. The tissue was illuminated through one of the most laterally positioned optodes, and sets of intensity measurements were collected at a ~75-Hz scan rate. For the slow hemodynamic-response measurement, measurements were performed using 30 optodes, in a 3×10 array positioned symmetrically about the midline of the occipital cortex. With each optode serving as both a source and a detector, a complete scan of the array required approximately 0.5 s.

The fast optical-response study (10 right-handed participants [6 female], 18-36 years old, mean age 26.6 yr) employed a target detection task. The visual information presented to the subjects consisted of a sequence of landscape scenes, most containing no artificial objects, while a small percentage, randomly placed within the sequence, included man-made transportation vehicles. The image presentation rate (PR) was either 4 Hz or 6 Hz, with data collected from each subject at both rates . The slow hemodynamic-response study (9 right-handed participants [2 female], 22-36 years old, mean age 27.6 yr) used a reversing-checkerboard (8 Hz) visual stimulus to induce an increase in neural activity in the visual cortex. The stimulus was presented for 2 s at a time, a total of 120 times, with a randomly varying time interval between presentations.

2.2 Data Analysis

For the fast optical-response experiment, data corresponding to each of the four wavelength-PR combinations were processed separately. For each combination, the data were frequency-filtered with a 2-30 Hz passband. Independent components were computed from each set of filtered data [24]. Any independent component (IC) that was significantly contaminated with cardiac-rhythm power, or was heavily weighted toward the superficial tissue layers, was deleted, and the remaining ICs were resummed to produce a set of artifact-cleansed time series. Block-average responses were computed for each subject's responses to images that did and did not contain man-made objects (T [*i.e.*, target] and NT [*i.e.*, non-target], respectively). Mann-Whitney tests were performed to determine which channels and time frames showed statistically significant T responses, NT responses, or T-NT differences. Within-

subject averages were computed over all channels yielding statistical significance for at least two time frames, and t-tests were performed to determine which time frames had a group-average response significantly different from zero.

In the slow hemodynamic-response case, 3D tomographic image time series Hb_{oxy} and Hb_{deoxy} were reconstructed, using the Near-infrared Analysis, Visualization and Imaging (NAVI) software package (www.nirx.net) [25]. The images were converted into ANALYZE format and exported to allow for additional processing using the AFNI image analysis suite (afni.nimh.nih.gov/afni/). Using AFNI, Hb_{total} was calculated by adding the Hb_{oxy} and Hb_{deoxy} time series. Every image-pixel time series was normalized to its temporal mean to compensate for any large differences in blood flow between individuals. The resulting scaled data were then analyzed as follows:

Area under curve. A deconvolution analysis was used to calculate an impulse response function (IRF) for the visual stimulus. The best-fitting gamma-variate function for this IRF was then determined using a nonlinear regression program [26]. This was used to calculate the event-related activation by expressing the area under the curve (AuC). To compare the AuC across participants, a t-test was performed, using a corrected voxel-level probability threshold of 0.05 ($p < 0.01$ individual voxel probability; 54-voxel cluster size). This provided a statistical test of the goodness of fit between the experimental manipulation and changes in Hb_{oxy}, Hb_{deoxy} and Hb_{total}, using standard techniques developed for the analysis of fMRI data. The correction for multiple comparisons was achieved by imposing a cluster-level threshold in addition to the voxel-level probability threshold. The cluster-level threshold, found using Monte Carlo simulations [27], was 54 contiguous voxels.

Time-fraction measures. For each voxel, the corresponding IRF was used to compute the fraction of time spent in each of the 6 combinatorial states (Table 1) over the 25 s following stimulus presentation. This resulted in a volume of the same dimensions as the reconstructed image, in which each voxel contains a number between 0 and 1 representing the fraction of time spent in one of the six states during the 25-s interval. Thus 6 volumes, one for each state, were computed for each participant. The statistical significance of the resulting time fractions was determined with t-tests comparing the observed time to a null hypothesis that was empirically determined by applying the same time-fraction analysis to images from each subject's baseline time interval.

3 Results

3.1 Measurement of Fast Optical Signal

The group-average differential T-minus-NT time course, derived from artifact-free ICs for the 830-nm, 6-Hz PR data, is plotted in Figure 1. Also included is a sketch of the measurement geometry, indicating the dimensions and coverage area of the detector array and the location of the illumination optode. Presentation of the stimulus begins at time 0 (vertical dashed line), and time frames for which the group-mean T/NT difference is statistically significant are marked with asterisks. The time delay between stimulus presentation and significant response is comparable to that typically found in electrical measurements of visual ERPs.

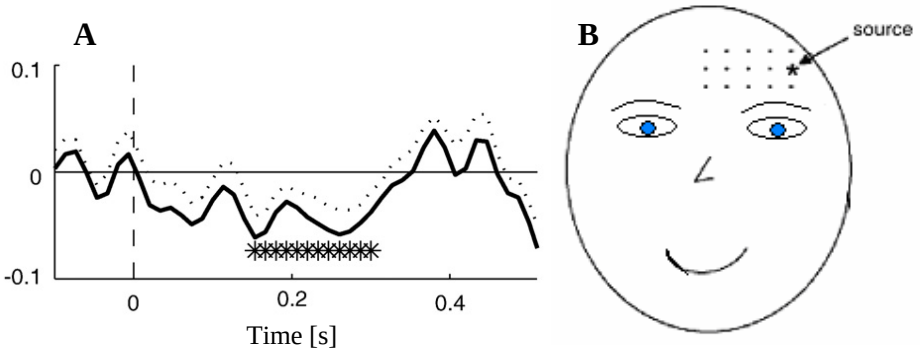

Fig. 1. Panel A: Normalized group-mean differential responses (target minus non-target) for the 830-nm, 6-Hz PR data. Dotted lines show standard errors for the corresponding signals at each time point; asterisks designate time bins with significant difference between targets and non-targets (t-test, $p < 0.05$). Panel B: geometry and location of the 15-optode array, with illumination site indicated.

3.2 Measurement of Slow Hemodynamic Response

Figure 2 shows two orthogonal sections through the center-of-mass of the region of activation, in response to the visual stimulus, identified by the group analysis of the participants' Hb_{oxy} AuC results. While many of the identified voxels are localized to the visual cortex, regions of activation outside of this location also were seen. The associated temporal response function (not shown) is triphasic, and its shape coincides

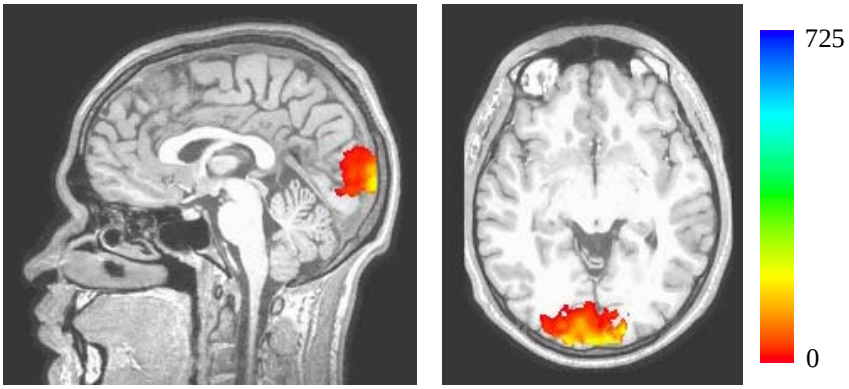

Fig. 2. Orthogonal sections through the center-of-mass of the region of activation identified by the group analysis of the participants' Hb_{oxy} AuC results.

well with the impulse response function seen in BOLD studies. Both the spatial- and temporal-domain results for Hb_{deoxy} and Hb_{total} are similar to those for Hb_{oxy}, while the size of the region identified as active is somewhat different in each case.

The time-fraction for each of the six combinatorial states was analyzed with a t-test across subjects that examined the difference between the fraction of time spent in

each state during the 25-s stimulation-response periods and during the baseline time interval. The same correction for multiple comparisons was performed here as was used in the AuC analyses. The results, as shown in Figure 3, were that only State 1 and State 4 were identified as undergoing significant event-related responses across all nine subjects. Fig. 3 shows that the spatial extent of the time-fractions associated

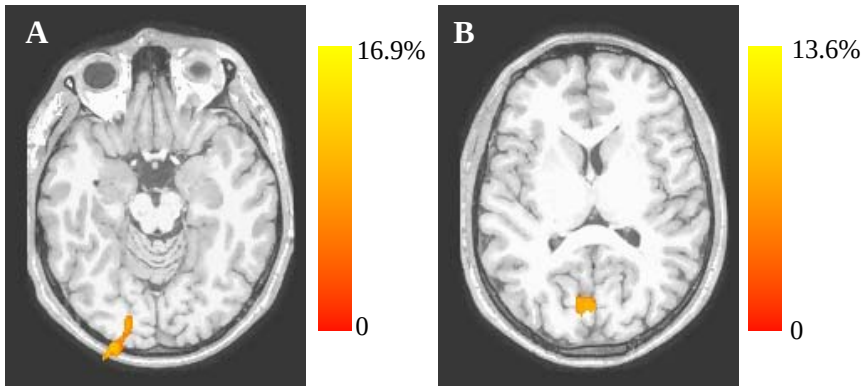

Fig. 3. Horizontal sections through the center-of-mass of the region of activation identified by the group analysis of the State 1 (Panel A) and State 4 (Panel B) time fractions.

with States 1 and 4 both are substantially smaller than those identified in the AuC analysis of any one Hb component. It is also seen that the State-1 and State-4 regions are centered in different locations, in both the Y (front-back) and Z dimensions. These results demonstrate that finer spatial resolution is achievable using analysis strategies that simultaneously consider multiple Hb components, and that differential information is associated with different combinatorial states.

4 Discussion

A research-and-development effort on functional NIRS imaging, under way since the late 1980s, seeks to identify and address all requirements for the sensing-technology associated with brain-computer interface systems. These include the ability to: 1) assess the location and magnitude of neural activity, either directly or through a surrogate parameter; 2) distinguish among different aspects of cerebral data processing (*e.g.*, sensory *vs*. cognitive); 3) examine tissue dynamics over a wide range of time scales/resolutions, with maximal freedom to specify the area being examined; 4) extract actionable, accurate information from a measurement, within a usefully brief time interval. For practicality, it also is necessary that the technology be as "transparent" as possible to the participants in a BCI application, and that it have a number of other qualities that can be classified as the "convenience" factor: ease of use, portability, ruggedness, successful performance in significantly non-ideal conditions, and low cost.

The bulk of our efforts for many years went into satisfying requirements 3 and 4 above, and into clearing the transparency and convenience hurdles, and this is sum-

marized in the Introduction. At the point that these criteria had been met, then it was appropriate to put serious effort into exploring requirements 1 and 2. The illustrative results presented here are an indication of our ability to isolate expected features of interest, strongly correlated with neural activity, from the NIRS signals generated by our technology. It is noteworthy that these encompassed measurements over two distinct cortical regions, and with very different temporal resolutions, source conditions, and data analysis strategies, but were accomplished with a single measuring platform.

Acknowledgments. This work was supported under grants 1R41NS050007-01 and 1R42NS050007-02 (RLB).

References

1. Barbour, R.L., Graber, H.L., Aronson, R., Lubowsky, J.: Model for 3-D optical imaging of tissue. In: Int. Geosci. and Remote Sensing Symp. (IGARSS), pp. 1395--1399. IEEE, Piscataway NJ (1990)
2. Aronson, R., Barbour, R.L., Lubowsky, J., Graber, H.L.: Application of transport theory to infra-red medical imaging. In: Operator Theory: Advances and Applications 51, 64--75. Birkhäuser Verlag, Basel (1991)
3. Barbour, R.L., Graber, H.L., Aronson, R., Lubowsky, J.: Imaging of subsurface regions of random media by remote sensing. In: SPIE Proceedings, Vol. 1431, pp. 192--203. SPIE Press, Bellingham WA (1991)
4. Barbour, R.L., Graber, H.L., Chang, J., Wang, Y., Aronson, R.: A perturbation approach for optical diffusion tomography using continuous-wave and time-resolved data. In: SPIE Institute of Medical Optical Tomography: Functional Imaging and Monitoring, pp. 87--120 (1993)
5. Graber, H.L., Chang, J., Aronson, R., Barbour, R.L.: A perturbation model for imaging in dense scattering media: derivation and evaluation of imaging operators. In: SPIE Institute of Medical Optical Tomography: Functional Imaging and Monitoring, pp. 121--143 (1993)
6. Schmitz, C.H., Löcker, M., Lasker, J.M., Hielscher, A.H., Barbour, R.L.: Instrumentation for fast functional optical tomography. Rev. Sci. Instrum. 73, 429--439 (2002)
7. Schmitz, C.H., Klemer, D.P., Hardin, R.E., Katz, M.S., Pei, Y., Graber, H.L., Levin, M.B., Levina, R.D., Franco, N.A., Solomon, W.B., Barbour, R.L.: Design and implementation of dynamic near-infrared optical tomographic imaging instrumentation for simultaneous dual-breast measurements. Applied Optics 44, 2140--2153 (2005)
8. Schmitz, C.H., Graber, H.L., Pei, Y., Farber, M.B., Stewart, M., Levina, R.D., Levin, M.B., Xu, Y., Barbour, R.L.: Dynamic studies of small animals with a four-color DOT imager. Rev. Sci. Instrum. 76, 094302 (2005)
9. Koizumi, H., Yamamoto, T., Maki, A., Yamashita, Y., Sato, H., Kawaguchi, H., Ichikawa, N.: Optical topography: practical problems and new applications. Applied Optics 42, 3054--3062 (2003)
10. Matsuo, K., Kato, T., Taneichi, K., Matsumoto, A., Ohtani, T., Hamamoto, T., Yamasue, H., Sakano, Y., Sasaki, T., Sadamatsu, M., Iwanami, A., Asukai, N., Kato, N.: Activation of the prefrontal cortex to trauma–related stimuli measured by near–infrared spectroscopy in posttraumatic stress disorder due to terrorism. Psychophysiology 40, 492—500 (2003)
11. Clark, C.R., Moores, K.A, Lewis, A., Weber, D.L., Fitzgibbon, S., Greenblatt, R., Brown, G., Taylor, J.: Cortical network dynamics during verbal working memory function. Int. J. Physophysiol. 42, 161--176 (2001)

12. Pei, Y., Graber, H.L., Barbour, R.L.: Influence of systematic errors in reference states on image quality and on stability of derived information for DC optical imaging. Applied Optics, 40, 5755--5769 (2001)
13. Pei, Y., Graber, H.L., Barbour, R.L.: Normalized-constraint algorithm for minimizing inter-parameter crosstalk in DC optical tomography. Optics Express 9, 97--109 (2001)
14. Graber, H.L., Pei, Y., Barbour, R.L.: Imaging of spatiotemporal coincident states by DC optical tomography. IEEE Trans. Med. Imag. 21, 852--866 (2002)
15. Barbour, R.L., Graber, H.L., Xu, Y., Pei, Y., Aronson, R.: Strategies for imaging diffusing media. Transport Theory Stat. Phys. 33, 361--371 (2004)
16. Graber, H.L, Xu, Y., Pei, Y., Barbour, R.L.: Spatial deconvolution technique to improve the accuracy of reconstructed three-dimensional diffuse optical tomographic images. Applied Optics 44, 941--953 (2005)
17. Xu, Y., Graber, H.L., Pei, Y., Barbour, R.L.: Improved accuracy of reconstructed diffuse optical tomographic images by means of spatial deconvolution: two-dimensional quantitative characterization. Applied Optics 44, 2115--2139 (2005)
18. Xu, Y., Pei, Y., Graber, H.L., Barbour, R.L.: Image quality improvement via spatial deconvolution in optical tomography: Time-series imaging. J. Biomed. Optics 10, 051701 (2005)
19. Xu, Y., Graber, H.L., Barbour, R.L.: An image correction algorithm for functional 3D DOT brain imaging. Applied Optics 46, 1693--1704 (2007)
20. Graber, H.L., Xu, Y., Barbour, R.L.: An image correction scheme applied to functional DOT scattering images. Applied Optics 46, 1705--1716 (2007)
21. Stone, J.V.: Independent Component Analysis: A Tutorial Introduction. MIT Press, Cambridge, MA (2004)
22. Stetter, M.: Exploration of Cortical Function. Kluwer Academic Publishers, Dordrecht (2002)
23. Barbour, R.L., Graber, H.L., Pei, Y., Schmitz, C.H., Di Martino, A., Castellanos, F.X.: Site-Specific Monitoring of Cerebral Vascular Hemodynamics with Dynamic Optical Tomography. Poster No. TH 252 at: Human Brain Mapping 2004
24. Laboratory of Computer and Information Science: Adaptive Informatics Research Centre, http://www.cis.hut.fi/projects/ica/fastica
25. Pei, Y., Wang, Z., Xu, Y., Graber, H.L., Monteiro, R., Barbour, R.L.: NAVI: A problem solving environment (PSE) for NIRS data analysis. Poster No. 114 at: Fifth Inter-Institute Workshop on Optical Diagnostic Imaging from Bench to Bedside at the National Institutes of Health (2006)
26. Garavan, H., Ross, T.J., Stein, E.A.: Right hemispheric dominance of inhibitory control: an event-related functional MRI study. Proc. Natl. Acad. Sci. USA 96, 8301--8306 (1999)
27. Ward, B.D.: Simultaneous Inference for FMRI DATA, http://afni.nimh.nih.gov/pub/dist/doc/manual/AlphaSim.pdf